Effect of pressure on hydrogen bonding in glycerol: A molecular dynamics investigation

Leslie J. Root and B. J. Berne
Department of Chemistry and the Center for Biomolecular Simulation, Columbia University, 3000 Broadway, New York, New York 10027

(Received 14 April 1997; accepted 4 June 1997)

We report results of a molecular dynamics study of liquid glycerol at the experimental density and at a series of elevated densities corresponding in our model to pressures of up to 0.7 GPa. We find that the degree of hydrogen bonding increases with increasing pressure over the range studied, and that the width of the hydrogen bond angle distribution increases with increasing pressure. The relevance to the experimental finding by Cook *et al.* [R. L. Cook, H. E. King, C. A. Herbst, and D. R. Herschbach, J. Chem. Phys. **100**, 5178 (1994)] that the fragility of glycerol increases with increasing pressure is discussed. © *1997 American Institute of Physics.* [S0021-9606(97)50734-3]

I. INTRODUCTION

Glycerol ($CH_2OHCHOHCH_2OH$) has been the subject of considerable and long-standing scientific interest.[1,2] It is an excellent glass former, and has been extensively studied experimentally[3,4] in connection with attempts to understand the nature of the glass transition. Glycerol is used in nature as a cryoprotectant[5] and has been the focus of study by researchers in cryopreservation.[6] In addition, the presence of three hydroxyl groups per molecule makes glycerol a particularly rich and complex system for the study of hydrogen-bonded fluids. Root and Stillinger have studied glycerol by molecular dynamics simulation of small systems (32 molecules), focusing on the structure of the liquid and amorphous solid[7] and the effects on the amorphous solid structure of energetic changes such as might accompany nonphotochemical hole burning.[8] Benjamin and co-workers[9] have used MD simulation to study scattering off liquid glycerol surfaces, in conjunction with experimental studies by Nathanson and co-workers.[10] In this paper we report a molecular dynamics investigation of hydrogen bonding in liquid glycerol and of the effects of pressure on the hydrogen bonding.

The complex nature of glycerol, which makes it such a fascinating subject for research, also makes it difficult to simulate. The existence of long- and short-ranged forces and a large variety of possible molecular conformations leads to important dynamics on a variety of timescales. The development of methods for handling multiple time scales accurately and efficiently, in particular the r-RESPA method,[11] makes it possible to study a system as complex as glycerol with much larger system sizes and longer timescales than was previously possible. Computer simulation is now a powerful tool for the study of structure and dynamics in glycerol.

The study is motivated in part by the experimental work of Cook *et al.*,[12] who studied the fragility of glycerol and other glass formers as a function of pressure. Fragility is a concept introduced by Angell[13] to classify glass formers. In strong glass-forming materials, such as network glasses, the viscosity exhibits a nearly Arrhenius dependence on temperature, indicating the predominance of a characteristic energy barrier in the material.[14] The viscosity of fragile glass-formers, such as *o*-terphenyl, shows a highly non-Arrhenius temperature dependence, indicating a broad distribution of energy barriers. Intermediate glass formers fall between these limits on an ''Angell plot'' of shear viscosity η vs $1/T$. At ambient pressure glycerol is an intermediate glass former. Cook *et al.*[12] report that glycerol becomes more fragile with increasing pressure, and point out that this behavior is consistent with a decrease in hydrogen bonding in glycerol with increasing pressure. That hydrogen bonding in glycerol would decrease with increasing pressure seems reasonable, since it is known[15] that in water hydrogen bonding decreases with increasing pressure. However, Marzke *et al.*[16] interpreted high pressure NMR chemical shift data for glycerol as indicating an increase in hydrogen bonding with increasing pressure. This also seems plausible. Crystalline glycerol is fully hydrogen bonded, with each molecule participating (as donor) in exactly three hydrogen bonds.[17] In the liquid each molecule participates in fewer than three intermolecular hydrogen bonds. In glycerol, unlike water, the crystal phase is denser than the liquid phase. Thus, one would expect that hydrogen bonding in glycerol would increase with increasing pressure, at least up to the crystal density. In the present work we explore the effect of pressure on structure and hydrogen bonding in liquid glycerol and suggest a possible resolution to this apparent conflict.

II. METHOD

A. General

The system studied consists of 256 glycerol molecules in a cubic box with periodic boundary conditions. The system was studied in the microcanonical ensemble at a series of fixed densities, with the average temperature approximately 298 K. At ambient pressure this is in the normal liquid region, since for glycerol $T_m = 291$ K and $T_g \approx 190$ K at 1 atm. At higher pressures the liquid is somewhat supercooled, since T_m increases with increasing pressure. Long-range, short-range, and intramolecular forces were treated on their respective time scales using r-RESPA.[11] Coulomb forces were treated by Ewald summation.

 0021-9606/97/107(11)/4350/8/$10.00

TABLE I. Lennard-Jones parameters for potential.

Pair	ϵ_{ij} (kcal/mol)	σ_{ij} (Å)
OH	0.09	1.80
OO	0.26	2.80
HH	0.26	2.45
CH	0.09	2.81
CC	0.09	4.10
CO (intra)	0.26	2.72
CO (inter)	0.26	3.50

B. Potential

The potential used is that developed by Root and Stillinger.[7] The model is fully flexible, with harmonic bond stretches and bond bends. CH_3 and CH_2 groups are treated in the united atom approximation. Hydroxyl hydrogens carry fixed partial charges of $+0.38e$, where e is the magnitude of the electronic charge, while oxygen atoms carry charges of $-0.38e$. Intramolecular Coulomb interactions are included, except between atoms covalently bonded to each other. All atom pairs interact via the Lennard-Jones potential except those covalently bonded to each other or to a common atom. We give the Lennard-Jones parameters here because the values of σ_{ij} for intramolecular and intermolecular CO pairs were inadvertently switched in the table of potential parameters in the earlier publication.[7] Table I gives the correct Lennard-Jones parameters, which were used in this work and in the earlier work. Coulomb interactions were treated by Ewald summation with $\alpha=0.22$ Å^{-1}, $|k|_{\max}=1.3$ Å^{-1}. The real-space contribution to the Ewald sum was truncated at $r_{\text{cut}}=13$ Å. Lennard-Jones interactions were summed over all atoms. These parameters gave energies accurate to $\mathcal{O}(10^{-5})$.

C. r-RESPA

Reversible RESPA has been discussed in several recent papers.[11,18–21] In the present work we use four time scales: that for intramolecular forces, short-range intermolecular forces, long-range intermolecular forces, and the forces due to the reciprocal-space part of the Ewald sum. The potential can be written as

$$V=V_{\text{intra}}+V_{\text{inter}}+V_{\text{recip}}. \tag{1}$$

Here, V_{intra} includes bond stretching, bond bending, and intramolecular LJ interactions, and the real-space part of the intramolecular contributions to the Ewald sum. V_{inter} includes intermolecular LJ interactions and the real-space part of the intermolecular contribution to the Ewald sum, and can be rewritten

$$V_{\text{inter}}=\tfrac{1}{2}\sum_{i=1}^{N}\sum_{j=1}^{N} v_{\text{inter}}(r_{ij}). \tag{2}$$

V_{recip} is the reciprocal-space part of the Ewald sum, including both inter- and intramolecular contributions. We approximate the propagator as

$$\begin{aligned} e^{iL\Delta t}\approx e^{iL_4\Delta t/2}&[e^{iL_3\delta t_3/2}[e^{iL_2\delta t_2/2}\\ &\times[e^{iL_1\delta t_1/2}e^{iL_0\delta t_1}e^{iL_1\delta t_1/2}]^{n_1}\\ &\times e^{iL_2\delta t_2/2}]^{n_2}e^{iL_3\delta t_3/2}]^{n_3}e^{iL_4\Delta t/2}, \end{aligned} \tag{3}$$

with

$$n_1\delta t_1=\delta t_2, \tag{4}$$

$$n_2\delta t_2=\delta t_3, \tag{5}$$

$$n_3\delta t_3=\Delta t, \tag{6}$$

and the Liouvillian given by

$$iL=iL_0+iL_1+iL_2+iL_3+iL_4. \tag{7}$$

Here

$$iL_0=\sum_{j=1}^{3N}\dot{x}_j\frac{\partial}{\partial x_j}, \tag{8}$$

$$iL_1=\sum_{j=1}^{3N}-\frac{\partial V_{\text{intra}}}{\partial x_j}\frac{\partial}{\partial p_j}, \tag{9}$$

$$iL_2=\sum_{j=1}^{3N}f_j^{\text{short}}\frac{\partial}{\partial p_j}, \tag{10}$$

$$iL_3=\sum_{j=1}^{3N}-\frac{\partial V_{\text{recip}}}{\partial x_j}\frac{\partial}{\partial p_j}, \tag{11}$$

$$\text{and}\quad iL_4=\sum_{j=1}^{3N}f_j^{\text{long}}\frac{\partial}{\partial p_j}, \tag{12}$$

with the intermolecular forces divided into short- and long-range parts as follows:

$$f_j^{\text{short}}=-\sum_{k=1}^{N}\sum_{\substack{l=1\\ l>k}}^{N}S(r_{kl})\frac{\partial}{\partial x_j}v_{\text{inter}}(r_{kl}), \tag{13}$$

$$f_j^{\text{long}}=-\sum_{k=1}^{N}\sum_{\substack{l=1\\ l>k}}^{N}[1-S(r_{kl})]\frac{\partial}{\partial x_j}v_{\text{inter}}(r_{kl}), \tag{14}$$

with the switching function given by

$$S(r)=\begin{cases}1, & r\leqslant r_c-\lambda,\\ 1+R^2(2R-3), & r_c-\lambda<r\leqslant r_c,\\ 0, & r>r_c,\end{cases} \tag{15}$$

where $R=[r-(r_c-\lambda)]/\lambda$. The following RESPA parameters must be optimized in this case: the time step Δt; n_1, n_2, and n_3; and the short-range cutoff r_c and healing length λ for each of the six types of atom pairs. In optimizing these parameters we required good energy conservation and stability, as measured by the quantity[22]

$$R=\frac{\sqrt{\langle E^2\rangle-\langle E\rangle^2}}{\sqrt{\langle KE^2\rangle-\langle KE\rangle^2}}. \tag{16}$$

We required $R\leqslant 0.007$, which has been found to give good results.[23] As will be discussed below, however, we found that parameters that gave very good energy conservation

nonetheless failed to give accurate results for the pressure. Accurate results for the pressure required somewhat larger short-range cutoffs r_c for the Coulomb interactions than were required for energy conservation. The optimized parameters, which gave $R \leqslant 0.007$ and pressures that agreed very closely with those calculated using the Verlet algorithm, are as follows: $\Delta t = 0.066\tau \approx 3.2$ fs; $n_1 = 3$; $n_2 = 4$; $n_3 = 1$; for LJ interactions $r_c = 2.5\sigma$, $\lambda = 0.65\sigma$; for Coulomb interactions $r_c = 6.2$ Å, $\lambda = 1.0$ Å; for interactions between charged atoms, which interact by both LJ and Coulomb forces, r_c is given by the larger of the LJ and Coulomb cutoffs, with the corresponding λ used. These parameters were found to give good results at all densities studied. Since the box length varied by less than 3% over the entire density range studied, it is not surprising that the same set of parameters was good for all densities. With these parameters we obtain a speedup with r-RESPA of a factor of 8 compared to velocity Verlet.

In this work we have used the ''force switching'' version of r-RESPA. We also explored using the ''energy switching'' technique introduced by Procacci and Berne,[19] separating the potential energy rather than the force into short- and long-range contributions. For the present system we had difficulty with the robustness of the algorithm using energy switching. Our difficulty was due to the fact that the switching function used, that given in Eq. (15) above, has discontinuities in the second derivative at $r_c - \lambda$ and r_c. The forces in the energy-switching algorithm involve the derivative of the switching function, and therefore the forces have discontinuities in slope at these points. The force-switching version of r-RESPA is both simpler to code and less sensitive to the switching function than the energy switching, and is therefore to be preferred except in cases where the energies are needed at intermediate r-RESPA time steps.[19] When energy switching is used, a switching function with continuous first and second derivatives at the endpoints should be used.

D. Evaluation of the pressure and compressibility

The pressure is given by[24,25]

$$P = \langle \mathscr{P} \rangle, \tag{17}$$

with

$$\mathscr{P} = \frac{N k_B \mathscr{T}}{V} - \frac{1}{3V}\,\phi. \tag{18}$$

Here, k_B is Boltzmann's constant and V is the volume of the unit cell. The temperature function is $\mathscr{T} = 2K/3Nk_B$, where K is the total kinetic energy. The virial ϕ is given by

$$\phi = \sum_{i=1}^{N_m} \sum_{j=1}^{8} k_j b_j^{(i)} (b_j^{(i)} - b_j^{(0)}) + \frac{1}{2} \sum_{i=1}^{N} \sum_{j=1}^{N}{}' \left[24\epsilon_{ij} \left(\frac{\sigma_{ij}}{r_{ij}} \right)^6 - 48\epsilon_{ij} \left(\frac{\sigma_{ij}}{r_{ij}} \right)^{12} \right] - V_{\mathrm{Coul}}. \tag{19}$$

Here, N_m is the number of molecules in the system, k_j is the bond stretching force constant and $b_j^{(0)}$ the equilibrium bond length of the jth bond in each molecule, and $b_j^{(i)}$ is the length of the jth bond on molecule i. The LJ parameters ϵ_{ij} and σ_{ij} are given above, and the prime on the second sum in the LJ term indicates that atoms covalently bonded to each other or to a common atom are excluded. V_{Coul} is just the Coulomb contribution to the potential energy, and is evaluated using Ewald summation as described above. We found that our initial r-RESPA parameters, which gave very good energy conservation, nonetheless gave results for the pressure that did not agree at all well with the Verlet results. The problem was found to be that with r-RESPA the OH covalent bonds were systematically shortened compared to their ''actual'' lengths, as calculated by Verlet with a timestep equal to the shortest r-RESPA time step. The error in the bond length was only $\mathscr{O}(10^{-4})$, which gave an error of about 3% in the bond-stretching contribution to the pressure. However, because the pressure is a sum of large terms that add to give a small result, a fairly small error in one term gives a very large error in the result. Thus the small error in the bond lengths resulted in pressures that differed from the Verlet results by as much as a factor of 10. Calculating the OH bond lengths, and thus the pressure, correctly required increasing the short-range cutoff r_c for the Coulomb interactions from 5 to 6.2 Å. Stuart *et al.*[18] report that the best results are obtained with r-RESPA when there is no systematic difference in the directions of the forces evaluated on different time scales. This appears to be the case in the present system as well—a larger short-range Coulomb cutoff is required so that the attractive and repulsive Coulomb contributions to the short-range part of the force are approximately balanced. Stuart *et al.*[18] find that breaking the Ewald sum into short-range and long-range parts, rather than real-space and reciprocal-space parts, yields a more efficient r-RESPA algorithm. In our system this alternative breakup of the Ewald sum yielded little speedup and did not improve accuracy, so for convenience we used the real-space/reciprocal-space breakup. With the larger short-range Coulomb cutoffs used, the pressures calculated using r-RESPA agree with those calculated using Verlet within a few percent.

As a check on the behavior at elevated pressures of the potential used, we also calculated the compressibility. The isothermal compressibility β_T is given by[24]

$$1/\beta_S = 1/\beta_T + TV\gamma_V^2/C_V, \tag{20}$$

with the adiabatic compressibility β_S given by[24]

$$1/\beta_S = \langle \mathscr{P} \rangle + \frac{2}{3}\frac{N}{V} k_B \langle \mathscr{T} \rangle + \frac{\langle \chi \rangle}{V} - \frac{V}{k_B T} \langle \delta \mathscr{P}^2 \rangle, \tag{21}$$

where

$$\chi = \frac{1}{9} \left[\sum_{i=1}^{N_m} \sum_{j=1}^{8} k_j b_j^{(i)} (2b_j^{(i)} - b_j^{(0)}) + 3 \sum_{i=1}^{N} \sum_{j=1}^{N}{}' \left(96\epsilon_{ij} \left(\frac{\sigma_{ij}}{r_{ij}} \right)^{12} - 24\epsilon_{ij} \left(\frac{\sigma_{ij}}{r_{ij}} \right)^6 \right) + V_{\mathrm{Coul}} \right] \tag{22}$$

and $\langle \delta \mathscr{P}^2 \rangle = \langle \mathscr{P}^2 \rangle - \langle \mathscr{P} \rangle^2$. In the above expression for the adiabatic compressibility we have taken advantage of the

fact that the Coulomb contribution to χ is simply equal to the Coulomb contribution to the potential energy. The Ewald sum therefore does not introduce any particular complication. Evaluation of the other contributions to β_S and β_T is messy but straightforward; expressions for the other quantities required are given in Allen and Tildesley.[24] The (classical) value calculated for C_V will be an upper bound on the actual (quantum mechanical) value, since at 298 K the stiff intramolecular vibrations of glycerol will not be thermally activated. Our calculated value for C_V is in fact substantially higher than the experimental value. However, we find that the second term of Eq. (20) is negligible in any case—the values of β_S and β_T are essentially identical. This is consistent with experiment[2]—experimental values for the adiabatic and isothermal compressibilities are identical to within the accuracy reported. Thus the error introduced by evaluating C_V classically does not affect our results for β_T. We found that the compressibility is subject to large fluctuations. However, the calculated compressibilities agreed fairly well with numerical estimates of the compressibility and with experiment.

E. Equilibration and run lengths

The system was started from an equilibrated structure obtained in previous work.[7] The density was adjusted in small increments by scaling the COM coordinates of each molecule, leaving intramolecular distances unchanged. The temperature was adjusted to 298 K by periodic rescaling of the translational, rotational, and internal velocities. Equilibration of total temperature, pressure, and translational, rotational, and internal temperatures was checked. Production runs were 3000 time steps, or 9.7 ps, and all properties examined were well converged in that time. To check that the system was not trapped in some atypical structure, we did the following: The sample at the highest density was heated in stages over 5 ps to 500 K, run at 500 K for 12.9 ps, then cooled in stages over 8.7 ps to about 298 K, and re-equilibrated at 298 K over 36.5 ps. During heating and cooling the density was adjusted so that the pressure stayed approximately constant throughout. After re-equilibration at 298 K a 3000-step production run was done. Results were essentially identical with those obtained before heating.

III. RESULTS AND DISCUSSION

A. Pressure and compressibility

The system was studied at approximately 298 K at a series of densities, ranging from the experimental density of 1.258 g/cc to a density of 1.38 g/cc, which corresponds in our model to a pressure of about 0.7 GPa. Cook *et al.*[12] report that at this pressure the shear viscosity η is about 30 times larger than that at ambient pressure. We felt that at higher densities, as dynamical processes become slower, special caution and perhaps special techniques would be required in any simulation study. The highest density studied was lower than the crystal density, which is 1.394 g/cc. The densities studied and the pressure calculated at each density are given in Table II. At the experimental density the model gave a negative pressure, so this density was not studied further. As may be seen from Table II, however, the model gives a pressure of 1 atm at a density quite close to the experimental density. Table II also shows the compressibility as calculated from Eq. (20), along with a numerical estimate of the compressibility calculated from the pressures at each two adjoining densities. As discussed above, the error bars on the calculated compressibilities are quite large, so the numerical estimate of the compressibility is more reliable. The agreement between the calculated value and the numerical estimate is reasonable, given the uncertainty in the calculated value. The experimental value[10] for the isothermal compressibility of glycerol at 28.5 °C and 1 atm is 2.1×10^{-5} atm^{-1}; the simulation results are in good agreement. The model also reproduces nearly quantitatively the experimentally observed decrease in compressibility with pressure.[2]

TABLE II. Simulation results for pressure and compressibility.

dens (g/cc)	T (K)[a]	P (atm)[a]	β_T (atm^{-1}), calc[b]	β_T (atm^{-1}), num[c]
1.258[d]		-919 ± 108		
1.28	298.1	38 ± 39	4.8×10^{-6}	
1.29	299.8	481 ± 46	5.4×10^{-6}	1.8×10^{-5}
1.30	297.6	1123 ± 29	9.5×10^{-6}	1.2×10^{-5}
1.35	300.5	4638 ± 76	6.4×10^{-6}	1.1×10^{-5}
1.38	300.7	6921 ± 67	5.5×10^{-6}	9.6×10^{-6}

[a]Average.
[b]Calculated using Eq. (20).
[c]Calculated using the values of P at each density and the next lower density.
[d]Experimental density at 298 K.

B. Pair correlation functions

The pressure dependence of the total pair correlation functions is difficult to sort out because of the difference in the way intermolecular and intramolecular distances vary with pressure. Intramolecular distances are essentially independent of pressure. For the intermolecular pcfs, hydrogen bond lengths are independent of pressure, while other intermolecular distances scale roughly with the box length L. We therefore calculated separately the intramolecular and intermolecular contributions to the pcfs. The intermolecular pcfs are given in Figs. 1 to 6. In Figs. 1 to 3, for atoms not directly involved in hydrogen bonding, distances are plotted in units of L. Intermolecular pair correlation functions for O and H atoms, which are involved in hydrogen bonding, are shown in Figs. 4 to 6, with distances plotted in Å. For clarity results are presented for only three of the densities studied. The intermolecular pcfs show that the intermolecular peak positions for peaks not involved in hydrogen bonding simply scale with L. Peaks corresponding to hydrogen bonding are enhanced at higher density, consistent with an increase in H bonding with pressure. This is confirmed by the H-bonding analysis, as reported below.

The intramolecular pcfs do not show substantial pressure dependence. Peak heights at $d=1.38$ g/cc are consistently somewhat smaller than those at $d=1.28$ g/cc. This is simply

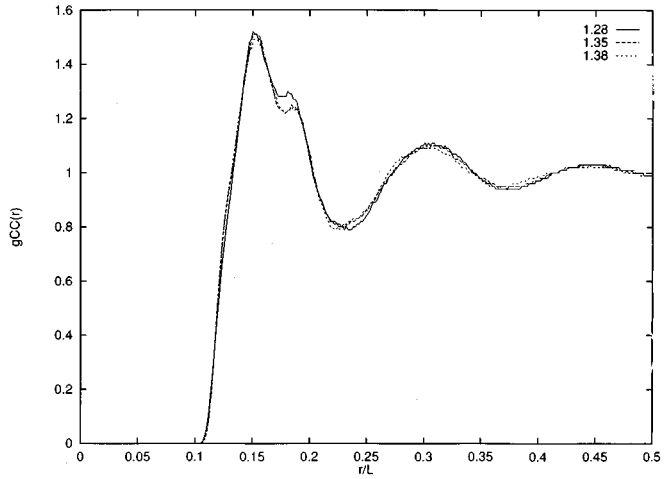

FIG. 1. Carbon–carbon pair correlation functions for intermolecular pairs. Curves are labeled with their densities, in g/cc. Note ''carbon atoms'' are actually united atoms.

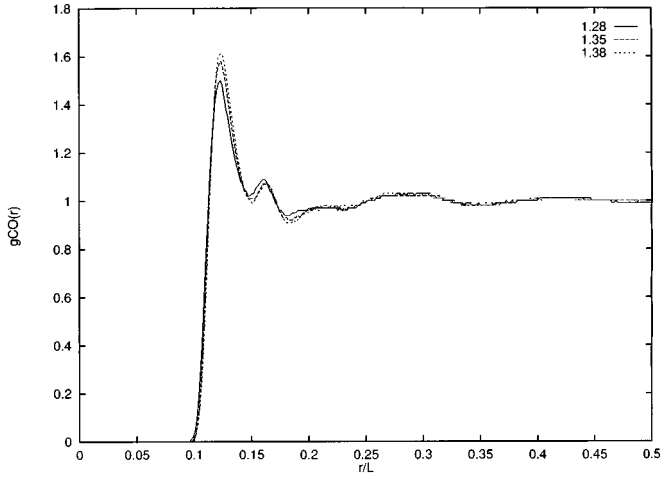

FIG. 3. Carbon–oxygen pair correlation functions for intermolecular pairs. Curves are labeled with their densities, in g/cc. Note ''carbon atoms'' are actually united atoms.

due to the density difference—since the number of intramolecular neighbors is independent of density, the peak heights must be smaller at higher densities. The intramolecular OH pair correlation function is shown in Fig. 7, with distance plotted in units of Å. The OH pcf shows essentially no change in the degree of intramolecular H bonding with pressure, and this is confirmed by the study of H bonding reported below. In addition, the distribution of intramolecular hydrogen bond angles is essentially independent of pressure. Thus no significant conformational changes are induced by pressure over the range studied.

C. Hydrogen bonding

The distance cutoff r_c (nonbonded O··H distance) for definition of a hydrogen bond was taken to be at the first minimum in the intermolecular OH pair correlation function which fell in the range 2.55 to 2.65 Å. We have taken $r_c = 2.55$ Å; results with $r_c = 2.6$ or 2.65 Å show the same trends as those reported here. The same cutoff distance was appropriate at all densities, since hydrogen bond lengths did not vary with pressure. We initially study all ''bonds'' with O··H distance less than the cutoff. Figure 8 shows the O–H··O bond angle distribution for intermolecular ''bonds'' at each density. It is clear that linear hydrogen bonds predominate, as they should, and that the distribution of bond angles is quite broad. Most significant, it is clear that the width of the bond angle distribution increases with increasing density. We believe that this accounts for the increase in fragility with pressure observed in Cook *et al.*'s experiments[12]—a broader distribution of bond angles means a broader distribution of bond strengths, which leads to greater fragility.

For further study of the hydrogen bonding we require a more meaningful definition of a hydrogen bond. From studying bond angles as a function of time we determined that

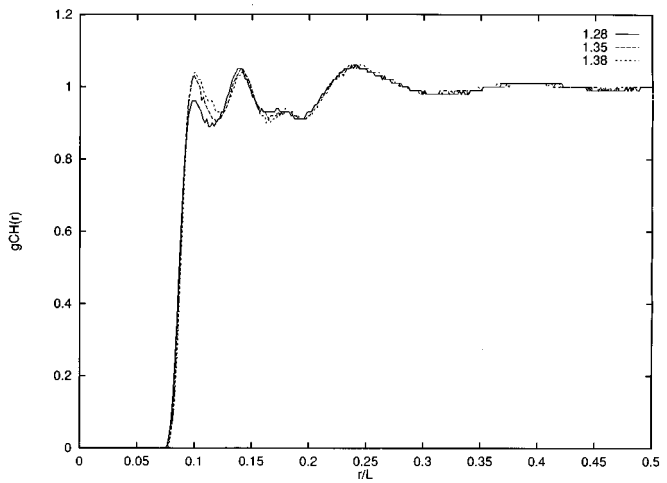

FIG. 2. Carbon–hydrogen pair correlation functions for intermolecular pairs. Curves are labeled with their densities, in g/cc. Note ''carbon atoms'' are actually united atoms.

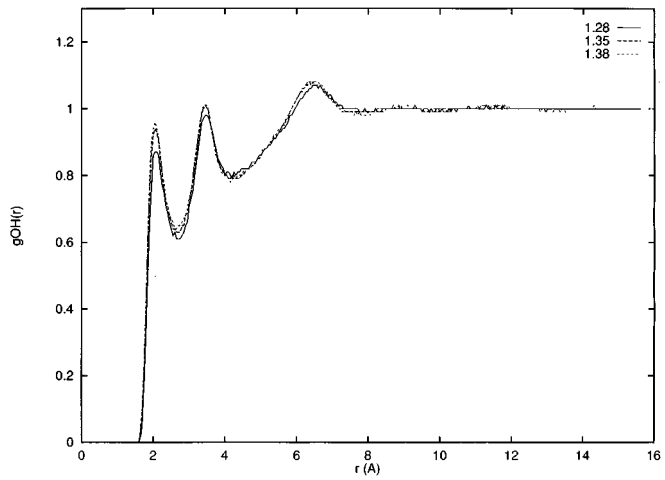

FIG. 4. Oxygen–hydrogen pair correlation functions for intermolecular pairs. Curves are labeled with their densities, in g/cc.

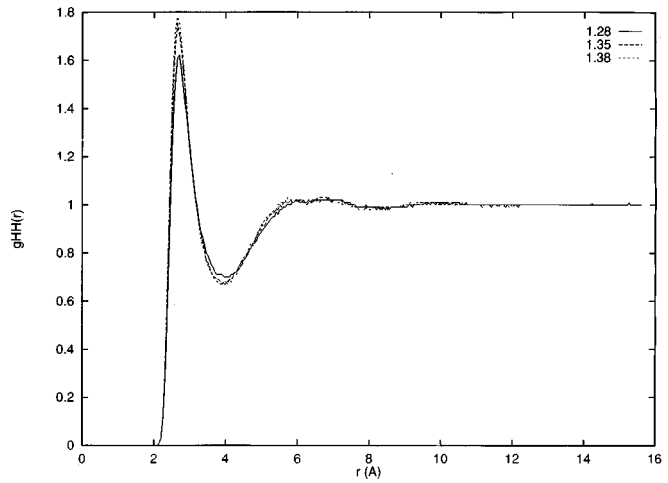

FIG. 5. Hydrogen–hydrogen pair correlation functions for intermolecular pairs. Curves are labeled with their densities, in g/cc.

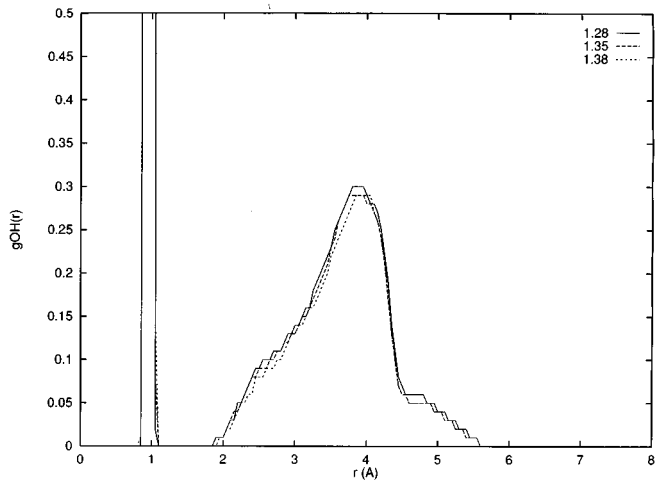

FIG. 7. Oxygen–hydrogen pair correlation functions for intramolecular pairs. Curves are labeled with their densities, in g/cc.

cutoffs for the hydrogen bond angle [O–H$\cdots$O angle] of $\phi_c = 35°$ to 45° were reasonable for intermolecular hydrogen bonds, in that they included most bonds that stayed intact but excluded most that were breaking or never really formed. We have chosen to use the most conservative criterion, $\phi_c = 35°$, but results with $\phi_c = 40°$ or 45° parallel those presented here. For intramolecular hydrogen bonds, which are necessarily quite bent and strained, a cutoff $\phi_c = 65°$ was found to be appropriate. For calculating the hydrogen bond lifetime we consider a bond to be formed when it exists with $r \leqslant r_c$ and $\phi \leqslant \phi_c$ for three consecutive data sets, and broken when it is missing for three consecutive data sets. (Data sets were recorded every ten time steps, or every 32.3 fs, so three consecutive data sets is about 0.1 ps.) The lifetime of each bond is defined to be the time from when it is first formed to when it's first broken. These criteria were determined from study of the hydrogen bond angles as a function of time. Sciortino and co-workers[26] have adopted a similar definition for hydrogen bond lifetimes in water. Luzar and Chandler[27] have used a more precise measure of lifetime in their detailed studies of hydrogen bond kinetics in water.

With the above criteria we calculated the average number of inter- and intramolecular hydrogen bonds at each density. We also defined a ''single'' hydrogen bond as an H atom that participates in only one, intermolecular, hydrogen bond, bonded to an O atom that participates in no more than two hydrogen bonds, with both intermolecular. These are the types of bonds that make up a strong hydrogen-bonded network. Bonds that do not fit this definition of ''single'' bonds are considered to be ''multiple'' bonds. ''Multiple'' bonds are necessarily fairly strained and weak. The average numbers of the various types of bonds are given in Table III. The number of intermolecular hydrogen bonds is found to increase significantly with density. Both the number of ''single'' bonds and the number of ''multiple'' bonds increases. The fractional increase in the number of multiple

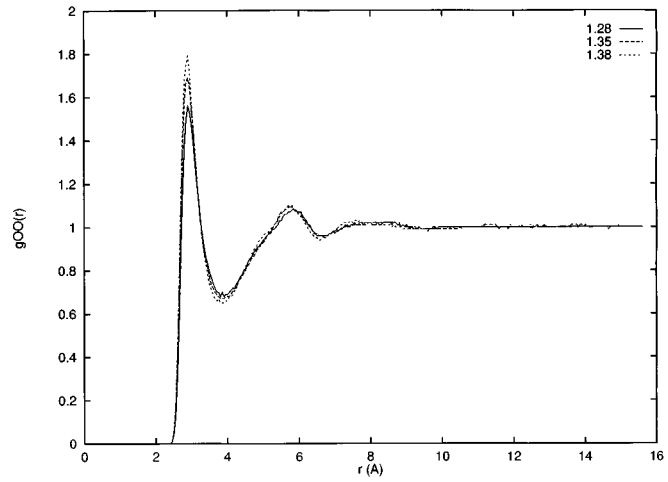

FIG. 6. Oxygen–oxygen pair correlation functions for intermolecular pairs. Curves are labeled with their densities, in g/cc.

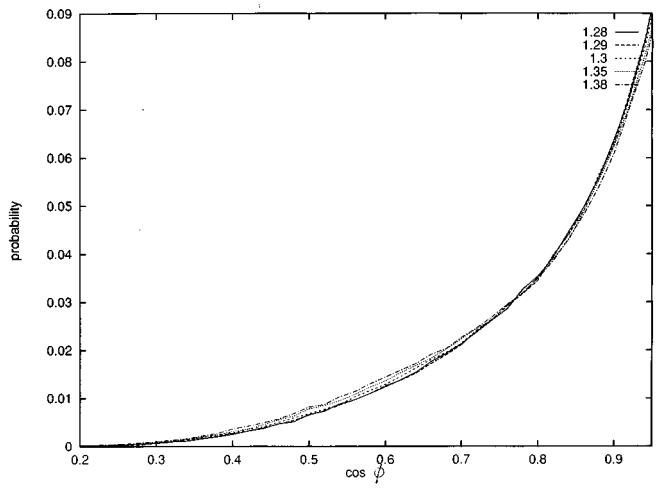

FIG. 8. Bond angle distribution for intermolecular hydrogen bonds. Curves are labeled with their densities, in g/cc.

TABLE III. Simulation results for hydrogen bonds: Average number of intermolecular, intramolecular, ''single,'' and ''multiple'' H bonds per molecule. See the text for definition of ''single'' and ''multiple'' bonds.

dens (g/cc)	# inter	# intra	# ''single''	# ''multiple''
1.28	1.63	0.08	1.48	0.12
1.29	1.68	0.08	1.51	0.14
1.30	1.68	0.09	1.50	0.15
1.35	1.79	0.09	1.60	0.15
1.38	1.84	0.08	1.65	0.15

bonds is greater than that in the number of single bonds, so that weaker bonds account for a larger fraction of the hydrogen bonds at higher density. This is consistent with the observed broadening of the bond angle distribution at higher density.

The number of intramolecular hydrogen bonds is independent of density. As discussed in an earlier paper,[7] in our model an isolated glycerol molecule adopts a closed-up conformation which permits it to form two intramolecular hydrogen bonds, albeit very bent and therefore very weak bonds. In the crystal the molecule adopts a more extended conformation which allows formation of three linear intermolecular H bonds, with no intramolecular bonds. In the liquid the extended conformation, with intermolecular H bonding, predominates, but some closed-up conformations with intramolecular H bonding are observed. The relative amounts of the two different conformations might be expected to be pressure-dependent, but the present results show that this is not the case—the number of intramolecular bonds is independent of pressure, over the range studied.

Hydrogen bond lifetime distributions are shown in Fig. 9. The hydrogen bond lifetime is not significantly affected by pressure, though there does seem to be a trend toward slightly longer lifetimes at higher densities. The hydrogen bond lifetime is about 1 ps, similar to that found in water.[26,27]

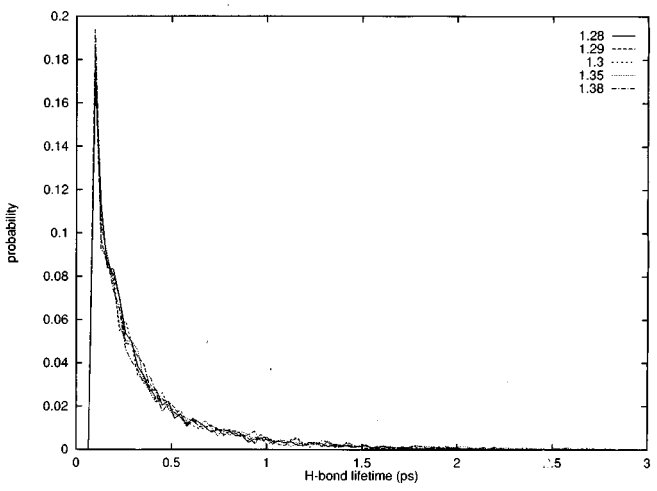

FIG. 9. Hydrogen bond lifetime distribution for intermolecular hydrogen bonds. Curves are labeled with their densities, in g/cc.

IV. CONCLUSION

We have used MD simulation with r-RESPA to study liquid glycerol at a series of five densities ranging from 1.28 to 1.38 g/cc, corresponding to a pressure range of 38 $\pm$39 atm to 6921$\pm$67 atm, or from about atmospheric pressure to 0.7 GPa. Over this pressure range we find that hydrogen bonding increases with increasing pressure. However, both the width of the H-bond angle distribution and the fraction of intermolecular H bonds that is ''multiple'' (bifurcated or trifurcated) also increase with increasing pressure. These results are consistent with the experimental results of Cook *et al.*,[12] who find that the fragility of glycerol increases with increasing pressure. Those authors suggest that the increase in fragility may be due to a decrease in hydrogen bonding. We find, however, that there is an increase in hydrogen bonding, but with a broader distribution of hydrogen bond angles and thus of bond strengths. This increase in the range of hydrogen bond energies would account for the observed increase in fragility.

ACKNOWLEDGMENTS

We would like to thank Dr. Steve Stuart, Dr. Steve Rick, and Dr. Piero Procacci for helpful discussions. This work was supported by a grant (to B.J.B.) from the National Science Foundation.

[1] J. W. Lawrie, *Glycerol and the Glycols: Production, Properties and Analyses* (Chemical Catalog Company, New York, 1928); A. R. Ubbelohde, *The Molten State of Matter* (Wiley, New York, 1978), Chap. 16.
[2] C. S. Miner and N. N. Dalton, *Glycerol* (Reinhold, Baltimore, 1953).
[3] W. T. Grubbs and R. A. MacPhail, J. Chem. Phys. **100**, 2561 (1994), and references therein.
[4] J. Wuttke, J. Hernandez, G. Li, G. Coddens, H. Z. Cummins, F. Fujara, W. Petry, and H. Sillescu, Phys. Rev. Lett. **72**, 3052 (1994).
[5] R. E. Lee, Jr., C.-P. Chen, and D. L. Denlinger, Science **238**, 1415 (1987); F. Franks, in *Water, A Comprehensive Treatise*, edited by F. Franks (Plenum, New York, 1982), Vol. 7.
[6] P. Mazur, Science **168**, 939 (1970); G. M. Fahy, D. I. Levy, and S. E. Ali, Cryobiology **24**, 196 (1987); Z. Chang and J. G. Baust, *ibid.* **28**, 268 (1991); G. Vigier and R. Vassoille, *ibid.* **24**, 345 (1987); P. Boutron and F. Arnaud, *ibid.* **21**, 348 (1984).
[7] L. J. Root and F. H. Stillinger, J. Chem. Phys. **90**, 1200 (1989).
[8] L. J. Root and F. H. Stillinger, Phys. Rev. B **41**, 2348 (1990).
[9] I. Benjamin, M. Wilson, and A. Pohorille, J. Chem. Phys. **100**, 6500 (1994); I. Benjamin, M. A. Wilson, A. Pohorille, and G. M. Nathanson, Chem. Phys. Lett. **243**, 222 (1995).
[10] M. E. Saecker and G. M. Nathanson, J. Chem. Phys. **99**, 7056 (1993).
[11] M. Tuckerman, B. J. Berne, and G. J. Martyna, J. Chem. Phys. **97**, 1990 (1992).
[12] R. L. Cook, H. E. King, C. A. Herbst, and D. R. Herschbach, J. Chem. Phys. **100**, 5178 (1994).
[13] C. A. Angell, Science **267**, 1924 (1995).
[14] F. H. Stillinger, Science **267**, 1935 (1995).
[15] R. L. Cook, H. E. King, Jr., and D. G. Peiffer, Phys. Rev. Lett. **69**, 3072 (1992).
[16] R. F. Marzke, D. P. Raffaelle, K. E. Halvorson, and G. H. Wolf, in *Second International Discussion Meeting on Relaxations in Complex Systems*, edited by K. L. Ngai (Alicante, Spain, 1993).
[17] H. van Koningsveld, Rec. Trav. Chim. **87**, 243 (1968).
[18] S. J. Stuart, R. Zhou, and B. J. Berne, J. Chem. Phys. **105**, 1426 (1996).
[19] P. Procacci and B. J. Berne, J. Chem. Phys. **101**, 2421 (1994).
[20] D. D. Humphreys, R. A. Friesner, and B. J. Berne, J. Phys. Chem. **98**, 6885 (1994).
[21] P. Procacci and M. Marchi, J. Chem. Phys. **104**, 3003 (1996).

[22] W. F. van Gunsteren and H. J. C. Berendsen, Mol. Phys. **34**, 1311 (1977).
[23] M. Watanabe and M. Karplus, J. Chem. Phys. **99**, 8063 (1993).
[24] M. P. Allen and D. J. Tildesley, *Computer Simulation of Liquids* (Oxford University Press, New York, 1987).
[25] T. Tominaga and S. Yip, J. Chem. Phys. **100**, 3747 (1994).
[26] F. Sciortino, P. H. Poole, H. E. Stanley, and S. Havlin, Phys. Rev. Lett. **64**, 1686 (1990); F. Sciortino and S. L. Fornili, J. Chem. Phys. **90**, 2786 (1989).
[27] A. Luzar and D. Chandler, Nature (London) **379**, 55 (1996); Phys. Rev. Lett. **76**, 928 (1996); J. Chem. Phys. **98**, 8160 (1993).